Electrical Engineering
https://doi.org/10.1007/s00202-025-03173-w

ORIGINAL PAPER

Enhancing efficiency and power quality in grid-connected photovoltaic systems based on linear matrix inequality methodology

Benameur Afif[1] · **Mohamed Salmi**[2] · **Mohammed Berka**[1] · **Umut Özkaya**[3]

Received: 9 May 2024 / Accepted: 12 May 2025

Abstract
This study presents an innovative control approach for enhancing the efficiency and power quality of grid-connected photovoltaic (PV) systems using linear matrix inequality (LMI) techniques. The primary objective is to develop a robust maximum power point tracking (MPPT) controller that ensures maximum energy extraction under varying solar irradiation conditions while improving the stability and reliability of power transfer to the grid. The system architecture comprises PV panels connected to a boost converter, managed by the LMI-based MPPT and a three-phase bidirectional converter that enables bidirectional power flow between the grid and the load. This work contrasts the performance of the proposed LMI method with the traditional sliding mode control (SMC), addressing the limitations of SMC, such as the chattering phenomenon and reduced efficiency under dynamic conditions. Key objectives include achieving superior power tracking accuracy, minimizing total harmonic distortion (THD) in the grid current, and ensuring smooth voltage regulation. Simulations demonstrate that the LMI-based MPPT controller delivers 2–3% higher power output compared to SMC across various solar irradiation scenarios, including rapid fluctuations and partial shading. The LMI methodology also significantly reduces THD by 20–30%, enhancing the power quality and ensuring compliance with grid standards. Additionally, the LMI control strategy eliminates the chattering effect observed in SMC, resulting in smoother control dynamics and improved system stability. These findings underscore the potential of the LMI approach to optimize energy harvesting, improve grid compatibility, and provide a reliable solution for modern PV systems, contributing to the advancement of sustainable energy technologies.

Keywords Linear matrix inequality · Maximum power point tracking · Sliding mode · Total harmonic distortion

Abbreviations

GSC	Grid side converter
INC	Incremental conductance
LMI	Linear matrix inequality
LQR	Linear quadratic regulator
MPPT	Maximum power point tracking
PV	Photovoltaic
P&O	Perturb and observe
PCC	Point of common coupling
PI	Proportional–integral
SMC	Sliding mode control
SM	Sliding mode
THD	Total harmonic distortions
VSC	Voltage source converters
VOC	Voltage-oriented control

✉ Mohammed Berka
m.barka@univ-mascara.dz

[1] Department of Electrotechnic, University Mustapha Stambouli of Mascara, Mascara, Algeria

[2] Department of Physics, University of M'sila, M'sila, Algeria

[3] Department of Electrical and Electronics Engineering, Konya Technical University, Konya, Turkey

1 Introduction

With the decrease in fossil fuel reserves and the increase in energy demand, it has been necessary to seek alternatives represented by renewable energy sources. On the other hand, this type of energy allows us to keep pace with the environmental challenges associated with the extraction and combustion of fossil fuels. These challenges include the disruption of ecosystems, contamination of air and water sources, and the release of greenhouse gases exacerbating climate shifts. For instance, an MPPT controller based on model predictive

Published online: 03 June 2025

control was evaluated in Ref. [1], showcasing their effectiveness in optimizing power output in PV systems. In Ref. [2], a back-stepping control technique was explored for standalone PV inverters, emphasizing its potential to improve energy conversion under variable conditions. Moreover, the authors of work in Ref. [3] introduced an adaptive model predictive controller to enhance the dynamic performance of PV systems, highlighting its ability to reduce steady-state oscillations caused by external disturbances. Meanwhile, the work proposed in Ref. [4] focused on LMI-based optimal linear quadratic controller designs for multiple solar PV units, emphasizing their role in stabilizing distribution networks. Also, the significance of sensorless field-oriented sliding mode control for PV-based induction motor drives has been demonstrated in Ref. [5], reinforcing the need for robust MPPT control under fluctuating load demands.

Comparing renewable energy sources to traditional fossil fuels reveals a number of benefits. Their abundance, sustainability, and zero-productions of greenhouse gases and other pollutants during their operation minimize their influence on the environment. Furthermore, the cost-competitiveness and economic viability of renewable energy technologies have increased, making them appealing choices for satisfying energy needs while lowering dependency on limited and environmentally damaging fossil fuels. The comparative study on grid-connected AC microgrids conducted in Ref. [6] with electric vehicle integration underlined the versatility and control flexibility offered by LMI methods. Other studies addressing the same issues with comparative analysis have been proposed in [7–10].

Given that photovoltaic systems are among the most promising energy sources, they attract attention. The following factors make them desirable: They use no fuel, produce no pollution, require less maintenance, and are noiseless. Despite the benefits, they add two key elements that influence the use of photovoltaic systems. Low conversion efficiency that is dependent on the climate and expensive installation expenses is these factors. One workable way to boost productivity is to implement maximum power point tracking, or MPPT [11–15]. These last strategies have been proposed recently to maximize the power output of photovoltaic systems under a range of irradiation scenarios, such as uniform, rapidly changing, or partially shaded environments. The two primary categories of MPPT approaches are direct techniques and indirect techniques.

The incremental conductance (INC) methodology and perturb and observe (P&O) technique are part of the direct approaches, which monitor the PV array's output voltage or current directly. While, indirect techniques include the sliding mode control (SMC) method, track and estimate the maximum power point using mathematical models and algorithms. In order to track the maximum power point, a model predictive control (MPC) algorithm combined with a P&O algorithm was applied in [1]. The obtained results were compared with traditional algorithms P&O and INC. The authors of the work published in [3] have been proposed a model to create an adaptive disturbance MPPT method based on a method similar to that used in [1]. This strategy tries to improve dynamic performance and reduce steady-state oscillations. It should be highlighted, too, that external disruptions might make it difficult to forecast future dynamic behaviors of system states and may lead to subpar dynamic responses. The need for a great number of regulation parameters to optimize control inputs is another MPC restriction that has been brought to light. As a result, this may reduce the flexibility of control synthesis. Because of these features, a linear quadratic regulator (LQR) controller based on linear matrix inequality (LMI) was developed for multiple PV modules interconnected in an array configuration rather than at the point of common coupling (PCC), and is designed specifically for voltage source converters (VSC). In terms of power delivery and minimizing total harmonic distortions (THD) of inverter output current, the LQR control unit was compared to a traditional proportional–integral (PI) controller. Given the results achieved in [4], it is noted that the photovoltaic panels were connected to the grid through only one stage without using a dc-link, which has of great importance in micro grids. The same features were obtained in [7], where MPC technology has been used to control the grid-connected inverter. A quick and efficient MPPT control method for PV systems is presented in papers [10, 16], which based on nonlinear techniques like sliding mode and back-stepping techniques. In [17], an effective H∞ controller employing LMI techniques has been introduced to manage a boost converter. While [10, 16, 17] offer advantageous features such as minimal tracking error, swift adaptability to solar radiation changes, and rapid transition responses, it is significant to note the fact the PV system under analysis consists of just one PV module that uses a converter to supply electricity to a resistive load so the system performance when integrated with the grid for assessing the quality of electrical power transmission was not evaluated.

To validate the effectiveness of the proposed method, extensive simulations were conducted under diverse operating conditions, including rapid fluctuations in solar irradiation and partial shading scenarios. The results indicate that the LMI-based MPPT controller consistently achieves 2–3% higher power extraction compared to the SMC approach, ensuring greater energy harvesting efficiency. Furthermore, the proposed method significantly reduces total harmonic distortion (THD) by 20–30%, enhancing power quality and ensuring better compliance with grid standards. Unlike SMC, which suffers from chattering effects that can introduce instability and energy losses, the LMI-based approach delivers smoother control dynamics and improved system stability.

Additionally, the method demonstrates superior adaptability to environmental changes, maintaining optimal power tracking with reduced oscillations. These advantages make the LMI-based MPPT controller a more reliable and efficient solution for grid-connected PV systems, contributing to enhanced energy conversion, improved grid compatibility, and long-term operational stability. The promising results highlight the potential of LMI techniques in optimizing photovoltaic performance and supporting the advancement of sustainable energy technologies.

The other sections of this manuscript with their titles and explanations are presented as follows: In Sect. 2, the general architecture is presented for the proposed system. Then in Sect. 3, a review of the model of the components of system with the necessary theoretical concepts is presented. In the same section, control systems were studied and designed, including the LMI-MPPT controller and the SM MPPT controller for controlling the boost converter, and the voltage-oriented control (VOC) methodology-based PI controller for controlling the converter connected to the grid. In Sect. 4, the simulation results are presented with discussions. In Sect. 5, a performance benchmarking analysis is presented to validate the results obtained based on our approach. Finally, the conclusion in Sect. 6 summarizes the obtained results.

2 Mathematical system model

2.1 Configuration of the proposed system

The suggested system's structure consists of the following.

1. PV panels.
2. Boost converter.
3. Resistance load.
4. Grid side converter (GSC).
5. Filter.

The proposed block diagram of the grid-connected PV system is depicted in Fig. 1.

2.2 PV model

PV panels, sometimes referred to as solar panels, are mostly composed of PV cells, which are formed of semiconductor materials like silicon. These cells are the main parts that use the photovoltaic effect to turn sunlight into electricity. PV panels also come with connectors for electrical connections, as well as support and protection elements to guarantee longevity and security. To accurately simulate the behavior of a PV cell, the electrical circuit model that is widely used to describe one usually consists of a number of electrical components. This model is illustrated in Fig. 2 [18, 19]. The mathematical model of PV cell is given as:

$$I_{pv} = [I_{sc} + k_I(T_c - T_{\text{ref}})]\frac{G}{1000} - I_D - \frac{V + IR_s}{R_{sh}} \tag{1}$$

Equation (1) represents the PV current where I_{pv} denotes the output current of the PV cell/panel. In the same Equation, I_{sc} denotes the short-circuit current at standard test conditions. Also, k_I, T_c, T_{ref}, G, and I_D denote the temperature coefficient of current, cell temperature, reference temperature (typically 25°C), solar irradiation (W/m^2), and diode current, respectively. On the other hand,V, I, R_s, and R_{sh} denote the PV cell voltage, PV cell current, series resistance, and shunt resistance, respectively. The diode current I_D is given as:

$$I_D = I_s\left\{\exp\left[\frac{e(V + IR_s)}{N_s AkT_c}\right] - 1\right\} \tag{2}$$

In Eq. (2), I_s, e, V, I, R_s, N_s, A, k, and T_c represent the saturation current, elementary charge (1.602×10^{-19} C), voltage across the diode, current through the cell, series resistance, number of cells in series, ideality factor of the diode, Boltzmann constant (1.381×10^{-23} J/K), and the cell temperature, respectively. The saturation current I_s is given by:

$$I_s = \left(\frac{I_{sc}}{\exp\left\{\frac{eV_{oc}}{N_s kAT_c} - 1\right\}}\right)\left(\frac{T_c}{T_{ref}}\right)^3 \exp\left\{\frac{e.E_g}{kA}\left[\frac{1}{T_{ref}} - \frac{1}{T_c}\right]\right\} \tag{3}$$

In Eq. (3), I_{sc}, V_{oc}, N_s, A, and E_g denote the short-circuit current, the open-circuit voltage, number of cells in series, ideality factor, and the energy band gap of the semiconductor, respectively. k, T_c, T_{ref}, and e are defined previously in the two Eqs. (1) and (2).

2.3 Boost converter model

The boost converter does play a key role in PV systems; the boost converter enables effective power transfer from the PV panels to the load or the grid. Its primary function is to efficiently increase the PV panel's voltage to match the requests of the load or the grid-connected inverter. The boost converter model used in this paper is depicted in Fig. 2; its dynamic model is provided below neglecting the current passing through the capacitor C_{pv} [20, 21]. The duty cycle for the boost converter is given as:

$$D = 1 - \frac{V_{pv}}{V_o} \tag{4}$$

In Eq. (4),V_{pv} and V_o represent the PV output voltage and the output voltage of the boost converter, respectively. The

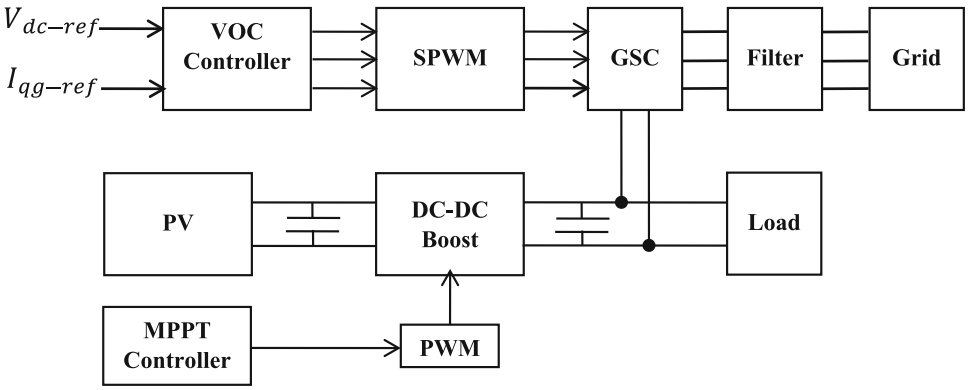

Fig. 1 Proposed block diagram of the grid-connected PV system

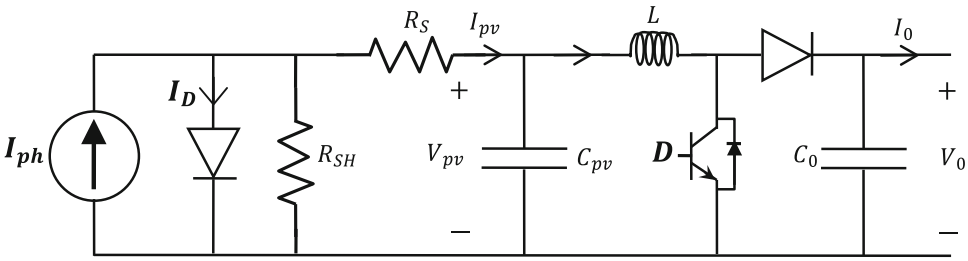

Fig. 2 Block diagram of PV cell connected to boost converter

current dynamics in the boost converter is expressed by:

$$\frac{\mathrm{d}I_{pv}}{\mathrm{d}t} = \frac{V_{pv} - V_o + DV_o}{L} \tag{5}$$

In Eq. (5), $\frac{\mathrm{d}I_{pv}}{\mathrm{d}t}$ and L denote the rate of change of PV current and the inductance of the boost converter, respectively. The voltage dynamics in the boost converter is expressed by:

$$\frac{\mathrm{d}V_o}{\mathrm{d}t} = \frac{I_{pv} - DI_{pv} - I_o}{C_o} \tag{6}$$

In Eq. (6), $\frac{\mathrm{d}V_o}{\mathrm{d}t}$ and C_0 denote the rate of change of output voltage and the Output capacitance of the boost converter, respectively.

2.4 Grid side converter model

The GSC which its structure is shown in Fig. 3 is located in the middle of both the grid and the PV system; it enables the power transfer from the grid to the load in the event of a decrease in the solar irradiation value, and the power transfer from the PV system to the grid otherwise.

Based on Fig. 3, the voltage balance equations for the converter can be written as follows [22].

$$\begin{cases} V_a - u_a = R_{\mathrm{rec}} i_a + L_{\mathrm{rec}} \frac{\mathrm{d}i_a}{\mathrm{d}t} \\ V_b - u_b = R_{\mathrm{rec}} i_b + L_{\mathrm{rec}} \frac{\mathrm{d}i_b}{\mathrm{d}t} \\ V_c - u_c = R_{\mathrm{rec}} i_c + L_{\mathrm{rec}} \frac{\mathrm{d}i_c}{\mathrm{d}t} \end{cases} \tag{7}$$

For the three columns (u_a, u_b, u_c), the converter voltages are established according to the state of the transistor switches and also based on the dc-link voltage. Eq. 8 can explain this feature.

$$\begin{bmatrix} u_a \\ u_b \\ u_c \end{bmatrix} = \frac{V_{dc}}{3} \begin{bmatrix} 2 & -1 & -1 \\ -1 & 2 & -1 \\ -1 & -1 & 2 \end{bmatrix} \begin{bmatrix} C_a \\ C_b \\ C_c \end{bmatrix} \tag{8}$$

The dc-link voltage relationship is given as follows.

$$\frac{\mathrm{d}V_{dc}}{\mathrm{d}t} = \frac{1}{C}\left(i_{dc-\mathrm{grid}} - i_{dc}\right) \tag{9}$$

where C_a, C_b, C_c denote pulses applied on transistors, $i_{dc-grid}$ denotes dc current on the gird side, i_{dc} denotes dc current on the side of the renewable generation system (inverter case) or from the load side (rectifier case), and i_c denotes the current of the capacitor.

The GSC can be represented in a $d-q$ frame as follows [23, 24].

$$V_{dg} = R_{\mathrm{filter}} i_{dg} + L_{\mathrm{filter}} \frac{\mathrm{d}i_{dg_{\mathrm{filter}}}}{\mathrm{d}t} - \omega_s L_{\mathrm{filter}} i_{gq_{\mathrm{filter}}} + u_{gd} \tag{10}$$

$$V_{qg} = R_{\mathrm{filter}} i_{qg} + L_{\mathrm{rec}} \frac{\mathrm{d}i_{qg_{\mathrm{filter}}}}{\mathrm{d}t} + \omega_s L_{\mathrm{filter}} i_{dg_{\mathrm{filter}}} + u_{gq} \tag{11}$$

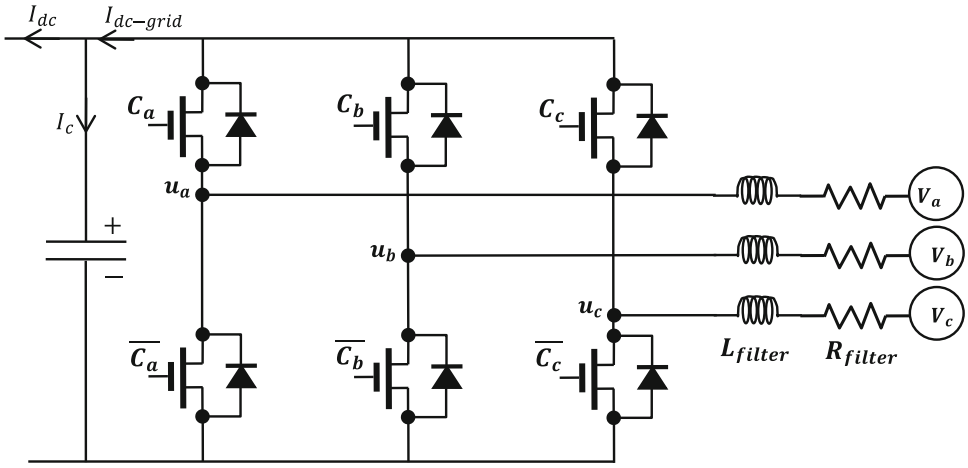

Fig. 3 Grid side converter presentations

3 Control systems design

3.1 MPPT control

PV panels typically convert only 12 to 25% of solar radiation into electrical power due to various factors including the efficiency of the solar cells, environmental conditions, and design limitations; in addition, it has a high initial cost. For these and other reasons, it is important to get the largest probable electrical energy from the panels. To increase the total amount of electric energy produced, researchers have explored various strategies, such as employing printed thin-film solar cells and implementing MPPT controllers. These technologies aim to improve efficiency and optimize the PV system performance. The MPPT controller dynamically regulates the boost converter operation to ensure that the PV panels produce their maximum power, thereby maximizing the power conversion efficiency.

3.2 SM MPPT controller design

The classical SMC method is considered to be a nonlinear algorithm which is based on the variable structure control methodology. Due to its crucial features, this method is often used. Perhaps the most important of these characteristics is performance efficiency against unmodeled dynamics and rejection of external disturbances. Robustness in the face of uncertainty in system parameters is one of its characteristics [25, 26]. The definition of the control law expression, which moves the state variables toward the sliding surface, is as follows [27].

$$u = u_{eq} + u_{sw} \tag{12}$$

The equivalent term u_{eq} represents the control action considered to drive the system to the sliding surface. It is responsible for ensuring that the system dynamics remain on this surface once it is reached. It is typically designed based on the system's dynamics and desired performance specifications. The switching term u_{sw} is essential for ensuring the attraction of the variable toward the sliding surface and meeting the convergence condition. It must be configured to eliminate the influence of any unexpected disturbance.

When $(\frac{dP}{dV} = 0)$ in PV systems, the (MPP) is reached. Thus, in order to use a SM MPPT controller, the sliding surface is selected in the manner described below.

$$S = \frac{\mathrm{d}P_{pv}}{\mathrm{d}V_{pv}} = \frac{\mathrm{d}\left(V_{pv}I_{pv}\right)}{\mathrm{d}V_{pv}} = 0 \text{ at the MPP} \tag{13}$$

The following equation must be solved in order to find the equivalent control term.

$$\dot{S} = \left[\frac{\mathrm{d}s}{\mathrm{d}X}\right]^T \dot{X} = 0 \tag{14}$$

The boost converter's equation can be expressed as follows using Eq. 5.

$$\dot{X} = \dot{I}_{pv} = \left[\frac{V_{pv} - V_o}{L}\right] + \left[\frac{V_o}{L}\right] D = F(X) + g(X)U_{eq} \tag{15}$$

So, the equivalent term U_{eq} is calculated by.

$$u_{eq} = 1 - \frac{V_{pv}}{V_o} \tag{16}$$

The switching term can be chosen as.

$$u_{sw} = k_{pv}S + Q_{pv}\mathrm{sign}(S) \tag{17}$$

The tuning constants k_{pv} and Q_{pv} of the SMC controller provide flexibility, which usually only has one tuning parameter. The selection and determination of these parameters will guarantee enhanced performance of the MPPT controller.

The control signal's ultimate expression is expressed by.

$$u_{pv}(t) = 1 - \frac{V_{pv}}{V_o} + k_{pv}S + Q_{pv}\text{sign}(S) \tag{18}$$

The Lyapunov function for stability analysis is provided as follows.

$$V(t) = 0.5S^2(t) \tag{19}$$

The following format can be used to express the stability condition.

$$S\dot{S} < 0 \tag{20}$$

By fixing Eq. 14, we find.

$$\dot{S} = \left(\frac{\text{dS}}{\text{d}I_{pv}}\right)\dot{I}_{pv} \tag{21}$$

The first term of Eq. 21 can be written as follows, where it can be noted that this term is always positive.

$$\left(\frac{\text{dS}}{\text{d}I_{pv}}\right) = \frac{\text{d}\left(\frac{\text{d}P_{pv}}{\text{d}V_{pv}}\right)}{\text{d}X} = \frac{\text{d}\frac{\Delta V_{pv} I_{pv}}{\Delta V_{pv}}}{\text{d}I_{pv}} = \frac{\Delta I_{pv}}{\Delta I_{pv}} > 0 \tag{22}$$

The following is a simplified version of the second term of Eq. 21.

$$\dot{I}_{pv} = \left(-\frac{V_o}{L}\left(1 - u_{pv}(t)\right) + \frac{V_{pv}}{L}\right) \tag{23}$$

$$\dot{I}_{pv} = \left(-\frac{V_o}{L}\left(1 - \left(1 - \frac{V_{pv}}{V_o} + k_{pv}S + Q_{pv}\text{sign}(S)\right)\right) + \frac{V_{pv}}{L}\right) \tag{24}$$

$$\dot{I}_{pv} = \frac{V_o}{L}\left(k_{pv}S + Q_{pv}\text{sign}(S)\right) \tag{25}$$

Lastly, the following form can be used to rewrite the stability condition in Eq. 20 by substituting the two Eqs. 21 and 25.

$$S\left(\frac{\text{dS}}{\text{d}I_{pv}}\right)\left(\frac{V_o}{L}\left(k_{pv}S + Q_{pv}\text{sign}(S)\right)\right) < 0 \tag{26}$$

If $\left(\frac{dS}{dI_{pv}}\right)$ is consistently positive, the stability requirement can be rewrite as follows.

$$S\left(k_{pv}S + Q_{pv}\text{sign}(S)\right) < 0 \tag{27}$$

Therefore, the values of the control parameters $k_{pv} and Q_{pv}$ must be negative. Figure 4 shows the block diagram of control system of SM MPPT controller.

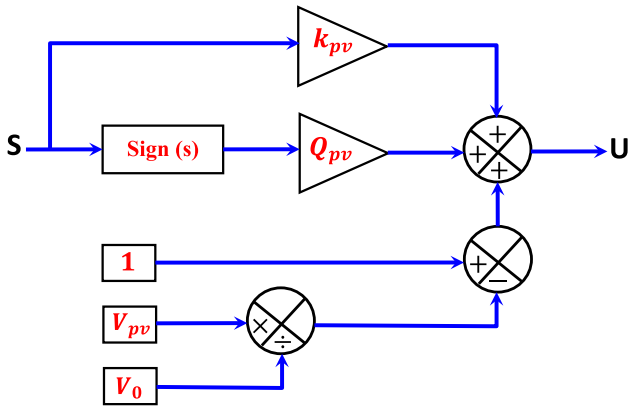

Fig. 4 Block diagram of the SM MPPT controller

3.3 LMI-MPPT controller design

3.3.1 LQR controller

The linear quadratic regulator (LQR) is an optimal control method where the weighting matrices R and Q play a crucial role in shaping system performance. The selection of weighting matrices R and Q in the LQR controller significantly affects system performance. The matrix Q penalizes deviations from the desired state, while R penalizes excessive control effort. A larger Q results in faster corrections but increases control energy, whereas a larger R ensures smoother control with reduced actuation effort. Typically, Q is chosen to emphasize critical state variables, such as voltage or current deviations, while R prevents aggressive control actions that may cause instability or actuator saturation. Selection methods include empirical tuning, normalization of state variables, or optimization techniques like genetic algorithms. The ideal balance depends on achieving fast response, minimal oscillations, and efficient energy use while maintaining system stability.

The objective of LQR issue is to create a linear control law for linear systems, which can be characterized by the subsequent connection. The proposed controller is an LQR scheme tuned using LMIs, its control law is derived by minimizing a quadratic cost function, its stability is guaranteed through a Lyapunov-based approach, and LMIs extend their robustness to handle uncertainties, ensuring enhanced and reliable performance in grid-connected PV systems.

$$y(t) = Cx(t) \tag{28}$$

$$\dot{x}(t) = Ax(t) + Bu(t) + \text{d}(t) \tag{29}$$

where $\text{d}(t)$ represents the external disturbance, $y(t)$ is the output signals, $u(t)$ is the input signals, and $x(t)$ is the state

variable vector. This linear control law is exploited to justify [11, 18].

1. The linear system is stabilized in accordance with Lyapunov condition.
2. Transferring the system between its starting and target states while reducing the performance indicator represented by the relationship below.

$$J = \int_0^\infty \left(X^T(t) Q X(t) + u^T(t) R u(t) \right) \mathrm{d}t \tag{30}$$

A linear quadratic regulator's linear control law can be described as follows.

$$u = -k_c X = -(1/R) B' P_c X \tag{31}$$

where P_c is the Lagrange variable which is a positive, semi-definite matrix, and can be finding by solving Riccati algebraic equation.

$$(A - Bk_c)' P_c + P_c(A - Bk_c) + k_c \prime R k_c + Q = 0 \tag{32}$$

The Key Insights are:

- The Lyapunov function $V(x) = x^T P x$ serves as a measure of system energy.
- The derivative $\dot{V}(x)$ is always negative, ensuring the system states decay over time.
- Since P, Q, and R are positive definite, the Lyapunov function is guaranteed to be valid.
- The solution of the Riccati equation ensures that P is always positive definite, reinforcing stability.

The application of the Lyapunov method in the LQR controller guarantees the global asymptotic stability of the closed-loop system. By solving the Riccati equation, the controller minimizes a cost function while ensuring that system trajectories do not diverge. The negative definiteness of $\dot{V}(x)$ confirms that the energy of the system always decreases, leading to a stable equilibrium.

3.3.2 LMI-based LQR controller

The LQR approach to calculating feedback constants may need to be modified in linear systems with uncertain models, where system parameters may fluctuate or remain unknown but within a certain range, or in the face of external disturbances. Instead, a methodology should be taken into consideration that emphasizes improving the system's performance in the presence of a change in the system's

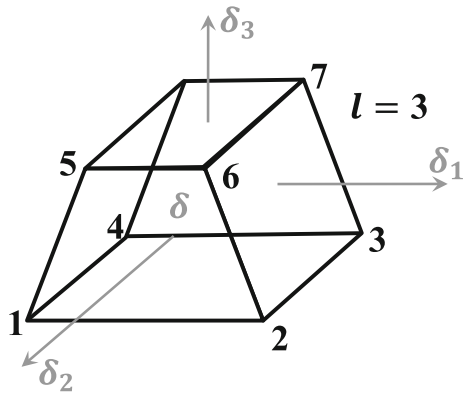

Fig. 5 Parameter variation space model (C)

parameters and overcomes the existing nonlinearity depending on LMI. This method stands out as a robust design tool that may be used to solve a widespread range of convex challenges [28, 29]. The standard LQR assumes a precisely known system model and optimizes performance by solving the algebraic Riccati equation (ARE), but it struggles with uncertainties and parameter variations, leading to potential instability. In contrast, the LMI-based LQR formulates the control problem as a set of linear matrix inequalities (LMIs), allowing explicit consideration of system uncertainties. LMIs provide a convex optimization framework, ensuring stability and robustness even under worst-case parameter variations. While standard LQR is computationally efficient but sensitive to inaccuracies, LMI-based LQR offers better robustness and flexibility, making it ideal for real-world applications with dynamic and uncertain environments.

The uncertainty systems can be expressed as.

$$\dot{x} = \left(\sum_{i=1}^{n} \lambda_i A^{(i)} \right) x + \left(\sum_{i=1}^{n} \lambda_i B^{(i)} \right) u \tag{33}$$

where $\sum_{i=1}^{n} \lambda_i = 1$

$$A^{(i)} = A_0 + \left(\sum_{j=1}^{l} A_j \delta_j^{(i)} \right) \tag{34}$$

$$B^{(i)} = B_0 + \left(\sum_{j=1}^{l} B_j \delta_j^{(i)} \right) \tag{35}$$

A_0 and B_0 denote the nominal state and input matrices, respectively. Additionally, let δ_j represent the scalar associated with the uncertain parameter corresponding to the uncertain matrices A_j and B_j.$\delta_j^{(i)}$ is the value of the parameter (j) in vertices (i) of space (C) whose axes are δ_j, l is the number of uncertainty parameters (Fig. 5).

Here, instead of searching for the value of P_c that satisfies the Riccati algebraic equation, we seek the value of P_c that satisfies the following inequality.

$$(A^{(i)} - B^{(i)}k_c)\prime P_c + P_c\left(A^{(i)} - B^{(i)}k_c\right) + k_c\prime R k_c + Q < 0 \tag{36}$$

where P_c is a positive definite matrix, and Q is some given matrix. However, solving this directly is not always straightforward due to the bilinear nature of the inequality. This form is not yet in LMI form because it involves the term P_c, which is typically not directly solvable in LMI frameworks. The Schurz complement is a mathematical tool that allows us to convert a bilinear matrix inequality (BMI) into a linear matrix inequality (LMI). If we define a new variable $S_c = {P_c}^{-1}$, and substitute $P_c = {S_c}^{-1}$, the inequality can be rewritten in an LMI form.

To obtain Eq. (37), we rewrite the original inequality in a form where we can apply the Schurz complement. The result is an equivalent linear matrix inequality, which can then be solved using LMI optimization techniques.

The inequality is now expressed in the standard LMI form, which are computationally solvable using convex optimization techniques.

$$\begin{bmatrix} A^{(i)}S_c + S_c{A^{(i)}}' + B^{(i)}N + N\prime B^{(i)} & N\prime & S_c \\ N & -R^{-1} & 0 \\ S_c & 0 & -Q^{-1} \end{bmatrix} < 0 \tag{37}$$

where $N = K_c S_c$

Here, the transition from Eq. (36) to (37) is based on the Schurz complement, a fundamental result in matrix theory that helps convert inequalities involving matrix inverses into linear matrix inequalities (LMIs), which are more convenient for computational solutions.

Accordingly, even with the uncertainty arising from the dead zone and the uncertainty arising from changing the system parameters, the control gain that attains good performance and stability of the system can be obtained based on the MATLAB programmer that uses the LMI code.

3.3.3 Affine/polytopic model of the boost converter

The boost converter's dynamic model can be expressed as a state space as follows, taking into account V_{pv} and I_o external disturbances.

$$\frac{\mathrm{d}I_{pv}}{\mathrm{d}t} = \frac{-V_o + DV_o}{L} \tag{38}$$

$$\frac{\mathrm{d}V_o}{\mathrm{d}t} = \frac{I_{pv} - DI_{pv}}{C_o} \tag{39}$$

The state variables (within some parts of Eqs. 38 and 39) were defined as uncertain parameters within a specific range from zero to nominal values to formulate the linear model of the system state space and then calculate the controller gain constants.

It can be seen that there is a coupling between the state variables and the input signal, so Eqs. 38 and 39 can be written as follows.

$$\frac{\mathrm{d}}{\mathrm{d}t}\begin{bmatrix} I_{pv} \\ V_o \end{bmatrix} = \begin{bmatrix} 0 & -\frac{1}{L} \\ \frac{1}{C_o} & 0 \end{bmatrix}\begin{bmatrix} I_{pv} \\ V_o \end{bmatrix} + \begin{bmatrix} \frac{\delta_1}{L} \\ -\frac{\delta_2}{L} \end{bmatrix} D \tag{40}$$

The values of $(\delta 1, \delta 2) \in (0 - V_o), (0 - I_{pv})$, respectively.

To enhance the MPPT controller performance and eliminate the steady-state error (SSE) in regulating the current I_{pv}, where the reference value I_{pv-ref} is obtained using the observer and disturbance algorithm shown in Fig. 6, an integrated procedure was added as a new state variable (ε) to the control system, so that the state space becomes as follows.

$$\frac{d}{dt}\begin{bmatrix} I_{pv} \\ V_o \\ \varepsilon \end{bmatrix} = \begin{bmatrix} 0 & -\frac{1}{L} & 0 \\ \frac{1}{C_o} & 0 & 0 \\ -1 & 0 & 0 \end{bmatrix}\begin{bmatrix} I_{pv} \\ V_o \\ \varepsilon \end{bmatrix} + \begin{bmatrix} \frac{\delta_1}{L} \\ -\frac{\delta_2}{L} \\ 0 \end{bmatrix} D + \begin{bmatrix} 0 \\ 0 \\ 1 \end{bmatrix} I_{pv-ref} \tag{41}$$

Figure 7 shows the block diagram of the LMI-MPPT controller.

3.4 Voltage-oriented control (VOC) of GSC

The two relationships below can be established for the electrical power passed by the GSC assuming that the d-axis applies to the electrical grid voltage vector ($V_q = 0$) [30].

$$P = 1.5V_{dg}i_{dg} \tag{42}$$

$$Q = -1.5V_{dg}i_{qg} \tag{43}$$

When the reference current value I_{gq-ref}, is set to zero, the relationship for the active power flowing through the GSC in the steady state can be expressed as follows, yielding a unit power factor.

$$P = 1.5V_{dg}i_{dg} = V_{dc}i_{dc-\mathrm{grid}} \tag{44}$$

Fixing the relationship of Eq. 21, we find.

$$i_{dc-\mathrm{grid}} = 1.5\frac{V_{dg}}{V_{dc}}i_{dg} \Longrightarrow i_{dc-\mathrm{grid}} = ai_{dg} \tag{45}$$

By fixing the relationship of Eq. 10, we find.

$$\frac{\mathrm{d}V_{dc}}{\mathrm{d}t} = \frac{i_{dc-\mathrm{grid}} - i_{dc}}{C} \tag{46}$$

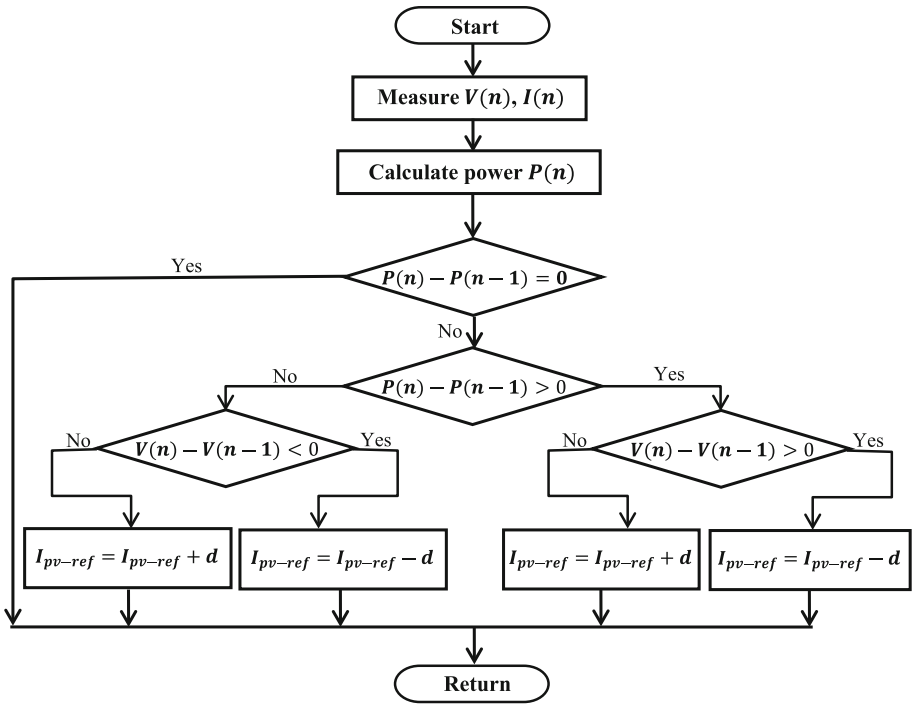

Fig. 6 Flowchart of the adapted P&O algorithm

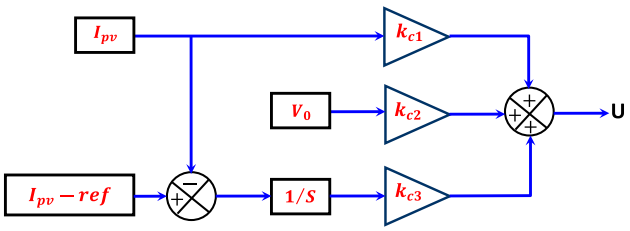

Fig. 7 Block diagram of the LMI-MPPT controller

Assuming that i_{dc} represents the external disturbance, the relationship 23 becomes.

$$\frac{\mathrm{d}V_{dc}}{\mathrm{d}t} = \frac{i_{dc-\mathrm{grid}}}{C} \tag{47}$$

Substituting the relationship 22 into the relationship 24, the following can be written.

$$\frac{\mathrm{d}V_{dc}}{\mathrm{d}t} = \frac{a}{C} i_{dg} \tag{48}$$

Thus, there are two regulating axes in the GSC control system.

1. On the q-axis, the current I_{gq} is controlled at zero.
2. The d-axis has two regulating loops: an internal regulating loop that regulates current id in accordance with the reference value established by the voltage regulating loop, and an external regulating loop that regulates dc-link voltage in accordance with the reference value.

Table 1 The number of panels used and the parameters of each panel

Parallel string	3
Number of panels per string	10
Maximum power (W)	213.15
Open-circuit voltage V_{oc} (V)	36.3
Voltage at maximum power point V_{mp} (V)	29
Short-circuit current I_{sc} (A)	7.84
Current at maximum power point I_{mp} (A)	7.35

The block diagram of VSC control system is presented in Fig. 8.

4 Simulation results

The parameters of panels are shown in Table 1.

The simulation outcomes are presented in this section, where it was assumed that solar radiation changes during the simulation period as shown in Fig. 9. The solar radiation is about 800 w/mˆ2 for the period spanned from 0 to 1s, and about of 1000 w/m^2 for the period from 1s until 3s, and about of 700 w/mˆ2 during period from 3s until 5s.

The energy consumed by the load is shown in Fig. 10, where it is noted that the load is disconnected from the source until the moment 2s, when the energy consumed in the load becomes 8500w. The usefulness of this feature is to test the

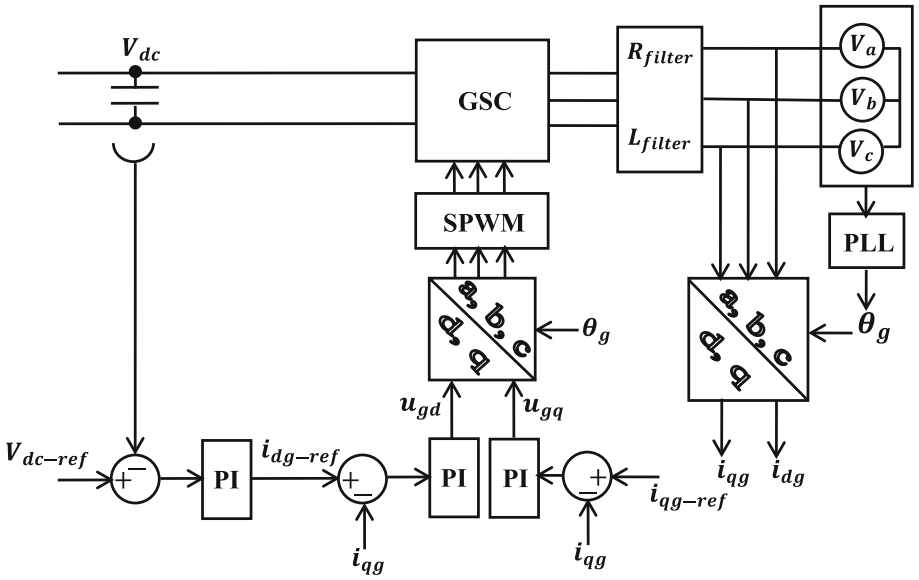

Fig. 8 Block diagram GSC control system

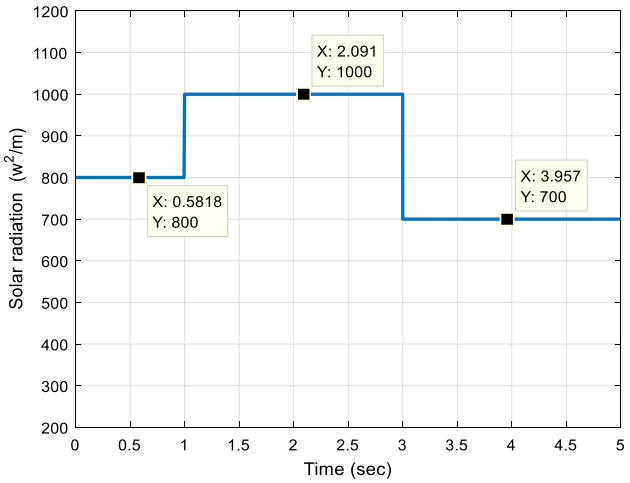

Fig. 9 Solar radiation changes during the simulation period

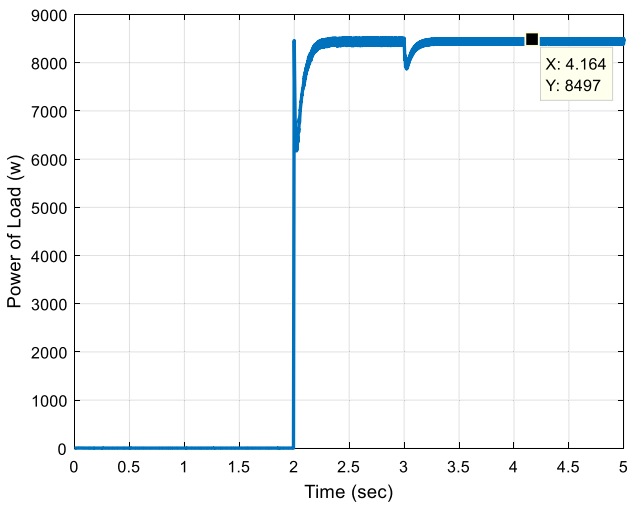

Fig. 10 Energy consumed by the load

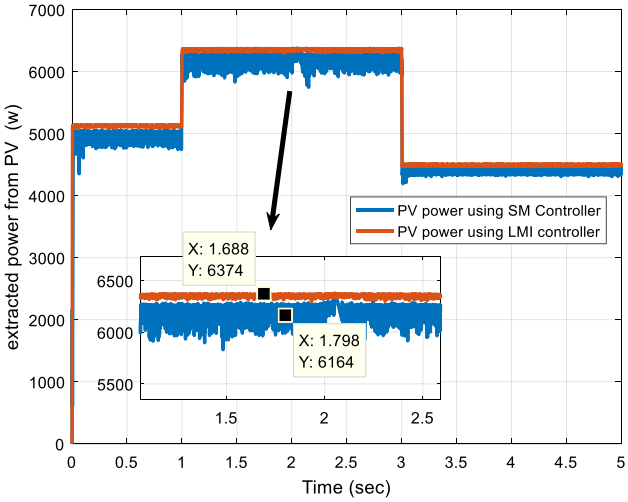

Fig. 11 The power extracted from photovoltaic panels for both proposed control approaches

performance of the system, so the grid side converter operates in inverter mode and rectifier mode.

Figure 11 shows the power extracted from photovoltaic panels for both proposed control approaches. Besides, the mutual power changes with the grid are shown in Fig. 12 and the response of the system to the regulation of the dc-link voltage is presented in Fig. 13. In Figs. 14 and 15 we observe the changes in the first phase current and the changes in the total harmonic distortion coefficient for the grid currents, respectively.

Figure 11 shows the superiority of the LMI methodology compared to the sliding mode methodology. The efficiency obtained is remarkable; this comes down to the extracted power which is always found to be higher in percentages

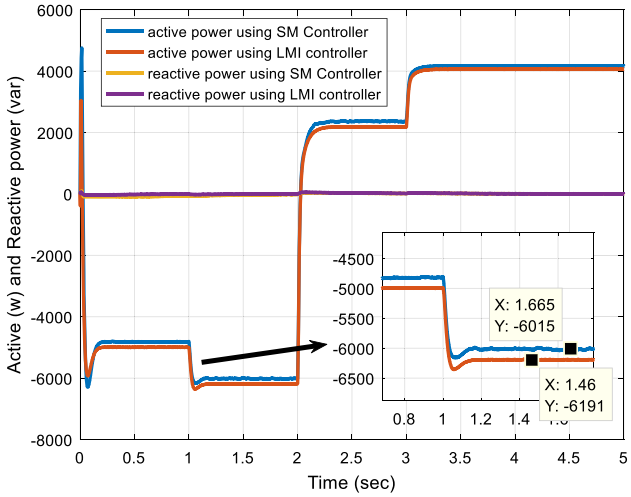

Fig. 12 Changes of power mutual with the grid

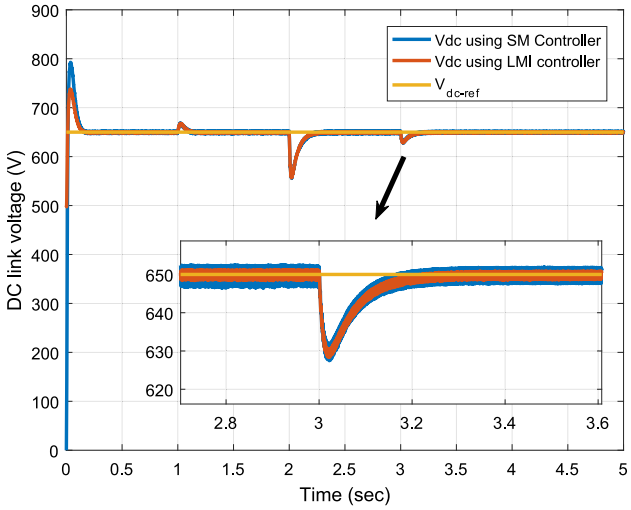

Fig. 13 System responses to regulation the dc-link voltage

between 2 and 3% for various scenarios that include different radiation values. It is also noted that it does not suffer from the chatter phenomenon that is observed when using the sliding mode methodology. The efficiency of using the LMI methodology also appears by observing Fig. 12, where the results show that the amount of power provided to the grid (the GSC acts as inverter) during the period from 0 to 2 s is greater compared to the sliding mode methodology where the solar radiation is at high value. It is observed that at the period of 2 to 5 s, the GSC acts as a rectifier, this comes down to solar radiation which has a low value. Consequently, the power provided by the photovoltaic panels is less than that consumed by the load. On the other hand, the amount of power consumed by the grid is less when using the LMI methodology. The effect of the chatter phenomenon when using SMC appears in the system's response to regulating the dc-link voltage, as it is observed from Fig. 13 that there is vibration the dc voltage. This has an influence on the current wave shown in Fig. 14, which has a lower harmonic distortion coefficient when using the SMC methodology shown in Fig. 15, where the harmonic distortion coefficient is 20 to 30% lower. The results drawn from this paragraph can be typesetting as shown in Table 2.

5 Performance benchmarking

In this section, we conduct a comprehensive performance benchmarking of the proposed approach against experimental works reported in recent literature, evaluating key performance metrics across power harvesting efficiency, total harmonic distortion (THD), control stability, and dynamic response.

Table 3 presents a comparative performance analysis of the proposed LMI-based MPPT approach against various control methodologies from prior research. The key performance metrics considered include power harvesting efficiency, total harmonic distortion (THD), control stability, and dynamic response. The LMI-based MPPT method demonstrates superior efficiency, achieving 2–3% higher power extraction than sliding mode control (SMC), while also significantly reducing THD by 20–30%. Compared to model predictive control (MPC) and back-stepping control, which require extensive tuning, the LMI approach ensures a smoother and more stable operation, effectively eliminating the chattering phenomenon associated with SMC. Furthermore, its performance in dynamic scenarios is comparable to adaptive MPC, which is known for its rapid adaptation but comes with increased computational complexity. Unlike H∞ control, which demands high computational resources, the LMI-based MPPT method offers a balanced trade-off between efficiency and implementation feasibility. The benchmarking results underscore the LMI approach as a robust and efficient control strategy for grid-connected PV systems, optimizing power extraction and ensuring grid compliance with minimal harmonic distortion.

Temperature has a significant impact on the electrical performance of photovoltaic (PV) panels and the efficiency of maximum power point tracking (MPPT) algorithms. As the temperature increases, the open-circuit voltage (V_{oc}) of PV cells decreases due to the reduction in the bandgap energy of the semiconductor material, leading to lower voltage generation. Although the short-circuit current (I_{sc}) slightly increases with temperature due to enhanced carrier generation, this increase is minimal and cannot compensate for the voltage drop, ultimately reducing the overall power output of the PV panel. Consequently, the maximum power point (MPP) shifts to a lower voltage, making it essential for MPPT controllers to adjust accordingly to maintain optimal power

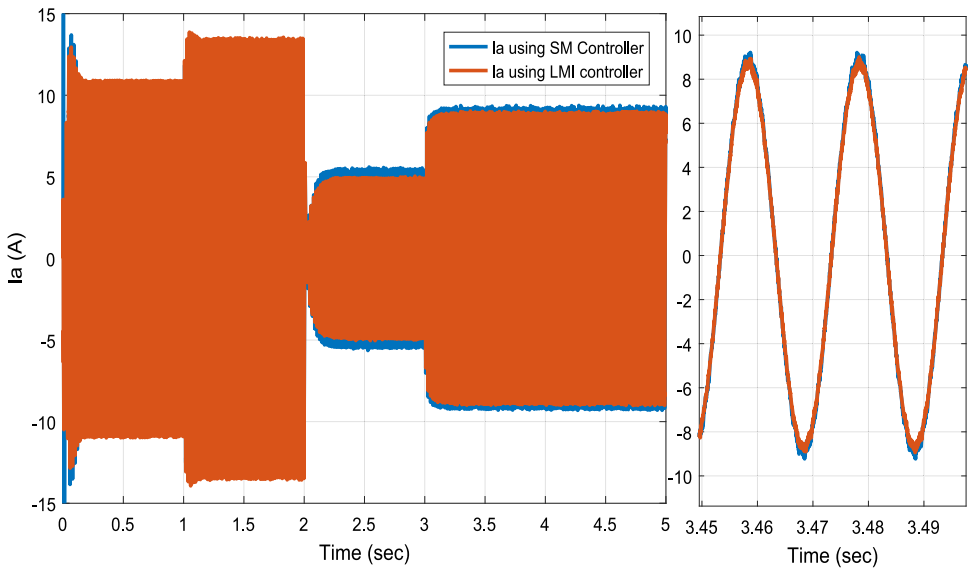

Fig. 14 Changes of first phase current

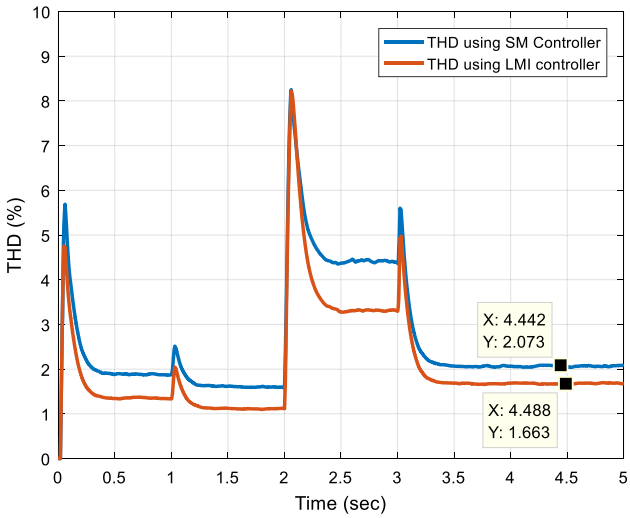

Fig. 15 Changes in the total harmonic distortion coefficient for the grid currents

extraction. However, many conventional MPPT techniques, such as perturb and observe (P&O) and incremental conductance (INC), may not respond effectively to these gradual temperature variations, leading to tracking inefficiencies and power losses. Additionally, rapid temperature fluctuations, caused by environmental changes such as passing clouds or wind cooling effects, can further challenge MPPT algorithms, causing increased oscillations and instability in power tracking. The efficiency of an MPPT controller depends on its ability to dynamically adapt to these variations while maintaining precise tracking of the MPP. If temperature changes are not adequately accounted for, the system may operate away from the optimal point, reducing energy yield and increasing total harmonic distortion (THD) in grid-connected systems. Therefore, evaluating MPPT methods under various temperature scenarios is crucial to ensuring robust and reliable performance across diverse environmental conditions, improving overall efficiency in solar energy harvesting.

6 Conclusion

This research successfully modeled and simulated a grid-connected photovoltaic (PV) system, demonstrating the advantages of the linear matrix inequality (LMI) methodology over the sliding mode control (SMC) approach. The proposed system included PV panels connected to a boost converter and a three-phase bidirectional converter for energy transfer between the grid and the load. The LMI-based maximum power point tracking (MPPT) controller consistently delivered 2–3% higher power output than SMC across varying solar irradiance levels, particularly under rapid changes in radiation. Moreover, it reduced the total harmonic distortion (THD) of the grid current by 20–30%, ensuring improved power quality. Unlike SMC, which suffers from the chattering phenomenon, the LMI approach provided smoother voltage regulation and stable power transmission, avoiding unnecessary fluctuations. During high solar radiation periods (800–1000 W/m^2), the LMI method transferred more power to the grid, while during lower radiation (700 W/m^2), it efficiently reduced power consumption from the grid. Notably, the power provided to the grid reached up to 6,374 W under high radiation, surpassing SMC, which delivered 6,164 W. The mutual power exchanged with the grid was optimized, with the LMI method consistently yielding lower power draw when acting as a rectifier. These findings underscore the LMI methodology's ability to enhance both the efficiency and stability of grid-connected PV systems, offering a more reliable and robust solution for maximizing solar energy utilization.

Table 2 Comparison results between LMI and SMC methodologies

	Controller				
Solar irradiation (w/m^2)	–	800	1000	1000	700
Load power (w)	–	0	0	8500	8500
PV power (w)	LMI	5127	6374	6374	4500
	SM	4975	6164	6164	4400
Mutual power with grid (w)	LMI	− 5000	− 6191	2190	4061
	SM	− 4821	− 6015	2362	4170
THD for grid current (%)	LMI	1.36	1.11	3.32	1.66
	SM	1.9	1.6	4.44	2

Table 3 Comparison of key metrics proposed approach with earlier works

Ref. no	Study/Method	Power Harvesting Efficiency	Total Harmonic Distortion (THD)	Control stability	Dynamic response
[31]	Model Predictive Control (MPC)	Good, optimized for steady state	Low THD, but requires tuning	Stable, but sensitive to parameter variations	Fast but needs tuning
[32]	Back-Stepping Control	Good efficiency, but complex	Moderate THD	Good, but computationally expensive	Moderate
[3]	Adaptive Model Predictive Control (AMPC)	High—Reduces oscillations	Very low THD	Stable, handles disturbances well	Very fast adaptation
[33]	LMI-Based Linear Quadratic Regulator (LQR)	High efficiency in multi-PV systems	Optimized for grid stability	Very stable under different loads	Smooth transitions
[34]	H ∞ Controller using LMI	High, optimized for noise rejection	Very low THD	high robustness	Fast but computationally expensive
This work	LMI-Based MPPT	2–3% higher than SMC	20–30% lower than SMC	High—Eliminates chattering effect	Smooth and fast

Despite these significant advancements, several areas remain for future exploration. One promising direction is integrating machine learning algorithms to enhance real-time adaptability in MPPT controllers. This could further improve the accuracy of power tracking under rapid environmental changes. Additionally, expanding the system's scope to incorporate hybrid renewable energy sources, such as wind or energy storage systems, may offer insights into achieving optimal power flow and greater grid resilience.

Acknowledgements This work was supported by the General Directorate of Scientific Research and Technological Development (DGRSDT), the body affiliated to the Algerian Ministry of Higher Education and Scientific Research.

Author contributions B.A. and M.S participated in data collection, analysis, and simulation, and wrote the main manuscript text, and M.B and U.O. wrote the main manuscript text and reviewing. All authors reviewed the manuscript.

Funding This research received no external funding.

Data availability All the data generated during and/or analyzed during the current study are available from the corresponding author on reasonable request.

Declarations

Conflict of interest The authors declare that they have no conflict of interest or competing interests.

Ethical approval This research study complied with the ethical standards.

Consent to participate Informed consent was obtained from all authors.

Consent for publication The authors confirm that there is informed consent to the publication of the data contained in the article.

References

1. Pradhan R, Panda A (2020) Performance evaluation of a MPPT controller with model predictive control for a photovoltaic system. Int J Electron 107(10):1543–1558

2. Diouri O, Es-Sbai N, Errahimi F, Gaga A, Alaoui C (2019) 2019, Modeling and design of single-phase PV inverter with MPPT algorithm applied to the boost converter using back-stepping control in standalone mode. Int J Photoenergy. 1:7021578
3. Metry M, Balog RS (2020) An adaptive model predictive controller for current Sensorless MPPT in PV systems. IEEE Open J Power Electron 1:445–455
4. Ghosh, S. K., Roy, T. K., Pramanik, M. A. H., Mahmud, M. A.: 2021, LMI-based optimal linear quadratic controller design for multiple solar PV units connected to distribution networks. In: 2021 IEEE Texas power and energy conference (TPEC) (pp. 1–6). IEEE.
5. Rai R, Shukla S, Singh B (2020) Sensorless field oriented SMCC based integral sliding mode for solar PV based induction motor drive for water pumping. IEEE Trans Ind Appl 56(5):5056–5064
6. Akarne Y, Essadki A, Nasser T, Laghridat H (2023) Modelling and control of a grid-connected AC microgrid with the integration of an electric vehicle. Clean Energy 7(4):707–720
7. Güler, N., & Irmak, E.: 2019, MPPT based model predictive control of grid connected inverter for PV systems. In: 2019 8th international conference on renewable energy research and applications (ICRERA) (pp. 982–986). IEEE.
8. Ullah Z, Wang S, Radosavljević J, Lai J (2019) A solution to the optimal power flow problem considering WT and PV generation. IEEE Access 7:46763–46772
9. Zhu R, De Carne G, Deng F, Liserre M (2017) Integration of large photovoltaic and wind system by means of smart transformer. IEEE Trans Industr Electron 64(11):8928–8938
10. Dahech K, Allouche M, Damak T, Tadeo F (2017) Back stepping sliding mode control for maximum power point tracking of a photovoltaic system. Elect Power Syst Res 143:182–188
11. MP A (2016) Linear quadratic optimal control of solar photovoltaic system: an experimental validation. J Renew Sustain Energy 8:5
12. Bakeer A, Salama HS (2021) Integration of PV system with SMES based on model predictive control for utility grid reliability improvement. Protect Control Modern Power Syst 6(2):1–13
13. Ali, A. I., Mohamed, E. E., Youssef, A. R.: 2017, MPPT algorithm for grid-connected photovoltaic generation systems via model predictive controller. In: 2017 nineteenth international middle east power systems conference (MEPCON) (pp. 895–900). IEEE.
14. Karanjkar DS, Chatterji S, Kumar A (2014) Design and implementation of a linear quadratic regulator based maximum power point tracker for solar photo-voltaic system. Int J Hybrid Inf Technol 7(1):167–182
15. Ahmed M, Abdelrahem M, Kennel R (2020) Highly efficient and robust grid connected photovoltaic system based model predictive control with Kalman filtering capability. Sustainability 12(11):4542
16. Ali K, Khan Q, Ullah S, Khan I, Khan L (2020) Nonlinear robust integral backstepping based MPPT control for stand-alone photovoltaic system. PLOS ONE 15(5):e0231749. https://doi.org/10.1371/journal.pone.0231749
17. Fard, M., Aldeen, M.: (2016) Robust control design for a boost converter in a photovoltaic system. In: 2016 IEEE 7th international symposium on power electronics for distributed generation systems (PEDG) (pp. 1–9). IEEE.
18. Batiyah, S., Zohrabi, N., Abdelwahed, S., Qunais, T., Mousa, M.: (2018), Optimal control design of a voltage controller for stand-alone and grid-connected PV converter. In: 2018 IEEE Texas power and energy conference (TPEC) (pp. 1–6). IEEE.
19. Khan R, Khan L, Ullah S, Sami I, Ro JS (2020) Back stepping based super-twisting sliding mode MPPT control with differential flatness oriented observer design for photovoltaic system. Electronics 9(9):1543
20. Priyadarshi N, Padmanaban S, Bhaskar MS, Blaabjerg F, Holm-Nielsen JB (2020) An improved hybrid PV-wind power system with MPPT for water pumping applications. Int Trans Electr Energy Syst 30(2):e12210
21. Bjaoui M, Khiari B, Benadli R, Memni M, Sellami A (2019) Practical implementation of the back stepping sliding mode controller MPPT for a PV-storage application. Energies 12(18):3539
22. Matiyali, K., Goel, S. K., Joshi, H.: (2019), Voltage oriented control of grid-tied solar PV system. In: 2019 women institute of technology conference on electrical and computer engineering (WITCONECE) (pp. 28–34). IEEE.
23. Ahiri, F. E., Chikh, K., El Afia, A., Lamterkati, J., Khafallah, M.: (2017), Simulation and experimental validation of VOC and hysteresis control strategies of unit power factor three-phase PWM rectifier. In: 2017 international conference on electrical and information technologies (ICEIT) (pp. 1–6). IEEE.
24. Aboudrar I, El Hani S, Heyine MS, Naseri N (2019) Dynamic modeling and robust control by ADRC of grid-connected hybrid PV-wind energy conversion system. Math Probl Eng 2019:1–19
25. Errami, Y., Obbadi, A., Sahnoun, S., Benhmida, M., Ouassaid, M., Maaroufi, M.: (2015), Design and sliding mode control for PMSG based wind power system connected to a non-ideal grid voltages. In: 2015 3rd international renewable and sustainable energy conference (IRSEC) (pp. 1–7). IEEE.
26. Sharma, S., Mishra, J. P., Datta, S.: (2015), Sliding mode power control of a DFIG based variable speed wind energy conversion system. In: 2015 annual IEEE India conference (INDICON) (pp. 1–6). IEEE.
27. Sayed, M. A., Youssef, A. R., Abdel-Wahab, M. N., Shabib, G.: (2015), Sliding mode control of variable speed wind energy conversion system based on five-phase PMSG for MPPT. In: The 17th international middle-east power system conference, Egypt.
28. Assunção E, Beteto MA, Teixeira MC, Silva ER (2018) Robust LQR-LMI state-derivative controller: a novel approach. 15th European workshop on advanced control and diagnosis. Springer International Publishing, Cham, pp 469–490
29. Zulkifli, N. N., Ramli, M. S.: (2021), state feedback controller tuning for liquid slosh suppression system utilizing LQR-LMI approach. In: 2021 IEEE international conference on automatic control & intelligent systems (I2CACIS) (pp. 52–57). IEEE.
30. Zhou X, Wang J, Ma Y (2020) Linear active disturbance rejection control of grid-connected photovoltaic inverter based on deviation control principle. Energies. 13(15):3790
31. Pradhan R, Panda A (2020) Performance evaluation of an MPPT controller with model predictive control for a photovoltaic system. Int J Electron 107(10):1543–1558
32. Diouri O, Es-Sbai N, Errahimi F, Gaga A, Alaoui C (2019) Modeling and design of single-phase PV inverter with MPPT algorithm applied to the boost converter using back-stepping control in standalone mode. Int J Photoenergy 2019:1–12
33. Ghosh SK, Roy TK, Pramanik MAH, Mahmud MA (2021) LMI-based optimal linear quadratic controller design for multiple solar PV units connected to distribution networks. IEEE Texas Power Energy Confer (TPEC) 2021:1–6
34. Fard, M., Aldeen, M.: (2016) Robust control design for a boost converter in a photovoltaic system. In: IEEE 7th international symposium on power electronics for distributed generation systems (PEDG), 1–9.